

DETERMINATION OF MECHANICAL PROPERTIES OF EXCISED DOG RADII FROM LATERAL VIBRATION EXPERIMENTS

INTRODUCTION

One approach to the noninvasive measurement of the mechanical properties of bones is to determine their vibration and wave transmission characteristics [1]. This approach presupposes however that we have a valid mathematical model which describes the dynamic behavior of whole bones in terms of their mechanical and geometric properties. For example, in slender, homogeneous, isotropic elastic beams a measurement of resonant frequencies for lateral oscillations provides information about the beam properties through the relation

$$f_n = \frac{1}{2\pi} \frac{K_n^2}{L^2} \sqrt{\frac{EI}{\rho A}} \quad (1)$$

where L is the length, EI the bending rigidity, and ρA the mass per unit length of the beam. The parameter K_n depends on the boundary conditions and the order of the mode of vibration [2]. Since whole bones are nonslender, inhomogeneous, anisotropic and viscoelastic their resonant frequencies are not correctly described by equation (1). The development of an appropriate mathematical description of lateral vibrations of whole bones can only be accomplished by a systematic comparison of theoretical and experimental analyses. The purpose of this paper is to provide some experimental data which can be used as a guideline in developing a mathematical model for whole bone vibrations.

EXPERIMENTS AND EQUIPMENT

Wet and dehydrated dog radii mounted in a cantilever configuration were subjected to static lateral loads and to free and forced lateral vibrations. The dog radii used in the experiments varied in length from 17.5 cm to 19.4 cm and were obtained from mongrel dogs of uncertain age. The bones were excised immediately after sacrifice of the animals and were stripped of excess soft tissue. To inhibit dehydration during excision and cleaning we applied periodically Ringer's solution. The cleaned bone specimens were then stored in Ringer's solution at a temperature of -20°C . Cantilever beam boundary conditions were ascertained by casting rectangular epoxy resin caps over the distal (wrist) ends of the radii and clamping the capped ends to a support. This boundary condition was chosen because it can be readily simulated in the laboratory and yields comparatively low resonant frequencies.

For all types of loadings the response of the bones was determined by measuring the temporal variation of the displacements of a discrete set of points along the bone. To this end a set of four electro-optical trackers were used (Physitech Models 39A and 440) which allowed contact-free sensing of the displacement patterns. The electro-optical trackers measure the motion of a target consisting of a line of contrasting light intensity (a white-black interface). By illuminating the bone from behind, the silhouette provided a natural target. Physically, each tracking system consists of an optical head unit and a control unit. Figure 1

shows the experimental arrangement with the optical axis of the trackers pointing across the bone surface towards the illumination source. The principal of operation of the optical trackers is shown in Figure 2. A lens on the optical head unit focuses an image of the target onto a photoemissive surface which converts the optical image into an electron image. The electrons are then accelerated toward a small aperture in front of a photomultiplier tube. Simultaneously, current is applied to a set of deflection coils which cause the electron image to sweep across the aperture. When the line of contrasting intensity in the image crosses the aperture the photomultiplier output current jumps and the control unit then samples the deflection coil current. Since the position of the electron image during the sweep is proportional to the deflection coil current the magnitude of this current provides a measure of relative target displacement. The current sample is then amplified and converted to a voltage proportional to the target displacement. Scanning (displacement sampling) is done at a 35 KHz rate for the Model 440 trackers and 50 KHz for the Model 39A's and the resolution and field of view (minimum and maximum measureable displacements) can be varied by using different lens combinations. Calibration of the tracking systems was achieved by moving the optical heads on a micrometer slide to record the output voltage vs. displacement.

Forced vibrations were induced by clamping the capped ends of the dog radii to the table of an MB Electronics Model C-10E shaker system which is capable of producing constant amplitude sinusoidal oscillations in the frequency range from 5 Hz to 3000 Hz. The maximum force rating of the shaker is 340 kg-force. With the combined system of the shaker and electro-optical trackers the displacements of both the table and bone could be determined in the frequency range from 5 Hz to 1000 Hz. Above 1000 Hz the amplitude of the table motion was too small to give a good signal to noise ratio using the optical trackers. The loading for static bending was applied by suspending a weight pan from a station near the free end of the bones. Free vibrations were produced by suspending a weight from the free end of the cantilevered bone and severing the suspension cord.

The displacement signals were displayed on a Tektronix RM-565 dual beam oscilloscope with a variable time delay feature. Forced vibration data was read directly from the CRT display by recording, for selected stations along the specimens, both the amplitude and phase of the motion relative to the shaker table motion. The phase angle between the two motions was determined by recording the corresponding delay time. For forced vibrations the excitation frequencies were determined using a Computer Measurements Company 706B electronic counter. In the static bending tests, the displacements were read directly from the oscilloscope display and for free vibrations single sweep photography was used.

EFFECTS OF INITIAL TWIST AND VISCOELASTICITY IN MACHINED "CONTROL" BEAMS

A mathematical description of the deformations of whole bones is complicated by inhomogeneity, anisotropy and viscoelasticity. Furthermore, estimation of the magnitude of each of these effects from experimental data for intact bones is difficult because they cannot be readily identified individually. In order to examine separately some of the effects of initial twist and viscoelasticity in vibrations of beams we have measured the bending vibration properties of "control" beams made of polymethylmethacrylate (pmm). This is a transparent plastic sold under the commercial names of Plexiglas, Lucite and Perspex. Figures 3 and 4 show the forced vibration response of an untwisted pmm cantilever beam in terms of an

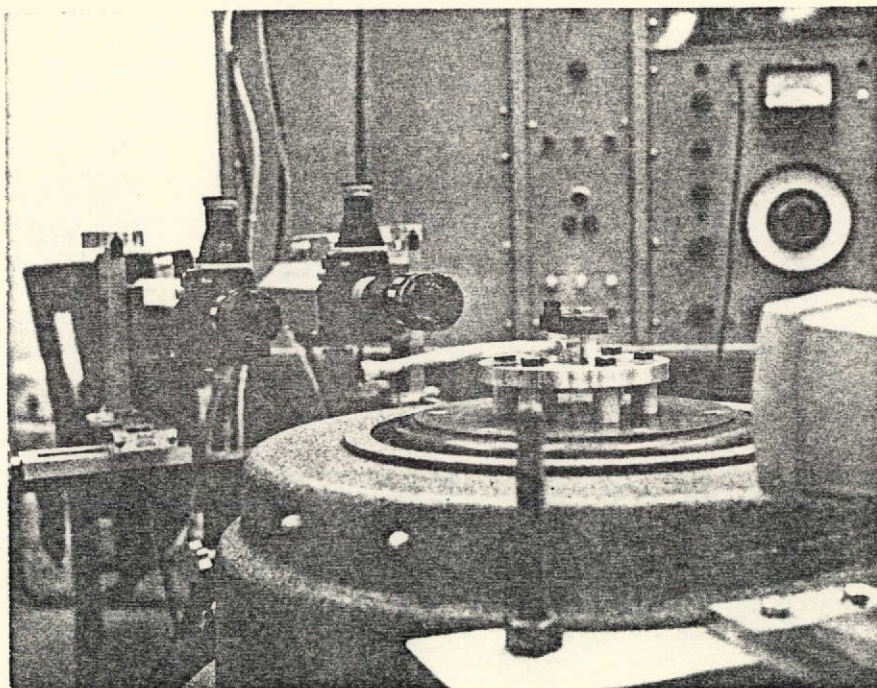


Figure 1. Forced vibration apparatus with (l. to r.) electro-optical tracking heads, dog radius mounted on shaker table and quartz-iodine lamp to provide an optical target of bone surface.

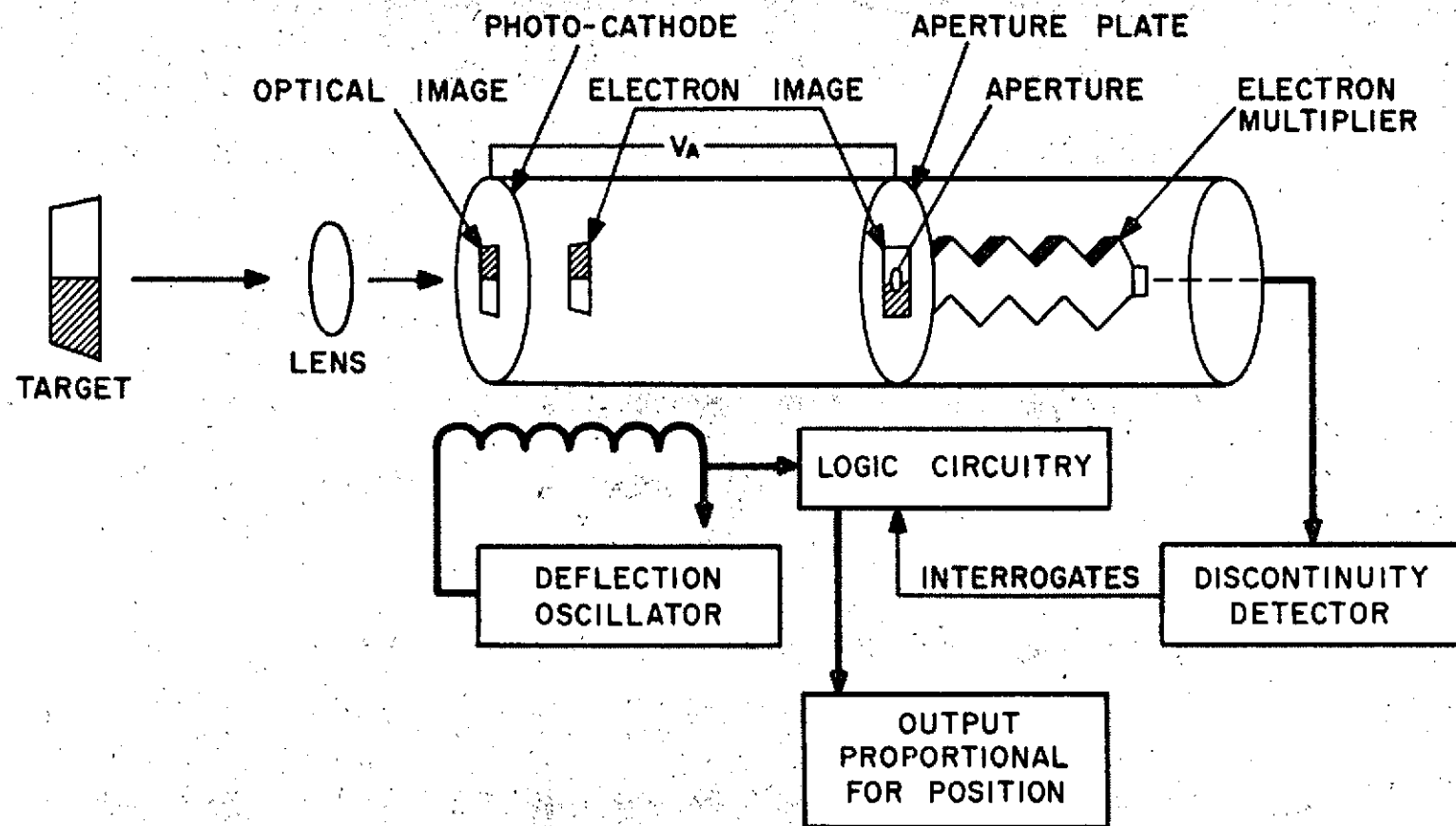


Figure 2. Principles of operation of the electro-optical tracking systems.

amplitude ratio and a phase angle. If $u(x, t)$ denotes the lateral displacement the amplitude ratio is defined by

$$\text{amplitude ratio} = \frac{|u(x, t)|_{\max}}{|u(0, t)|_{\max}}$$

where x is directed along the longitudinal axis of the beam with its origin at the clamped end. The phase angle is the difference in phase between motions at the station x along the beam and the motion of the clamped end. Figure 3 shows the amplitude ratio and phase relations for the station $x/L = 0.98$ (L is the length of the beam) as functions of frequency. The first three resonant frequencies, i.e. the frequencies at which maximum amplitudes are obtained, are 28, 182 and 520 Hz. The spatial variations of the amplitude ratio and phase for these resonant frequencies are shown in Figure 4. Note that the amplitude ratio distributions do not actually represent the deformation pattern at a particular time because for different stations the maximum displacement occurs at different times. For this pmm beam the ratios of the second and third resonant frequencies to the first are 6.5 and 18.6 respectively. In an elastic cantilever beam whose resonant frequencies are given by equation (1) the corresponding ratios are 6.27 and 17.55 respectively. The discrepancy indicates that Young's modulus for the pmm beam used increases with frequency. Before examining further the variations in Young's modulus with frequency we shall first investigate the effects of initial twist on the resonant frequencies.

A beam has initial twist if the principal directions of the cross sections vary when moving along the beam length. An examination of the effects of initial twist is important for vibrations of whole bones because many bones can be expected to have some initial twist. The response of an initially twisted pmm beam is shown in Figures 5 and 6. This beam was constructed such that the rate of twist along the beam was approximately constant and the total twist at the end was 100 degrees. The cross section was rectangular with thickness h and width b such that the ratio of principal moments of inertia was $I_2/I_1 = 2.25$. This ratio approximately corresponds to the value for a dog radius. Figure 5 shows the amplitude ratio and phase as a function of frequency for a station near the free end ($x/L = 0.96$). The beam was vibrated such that at the clamped end we had only lateral motion in the principal direction for which the bending rigidity was lowest. The amplitude ratios shown in Figures 5 and 6 correspond to the displacement components in the direction of the support vibration. The arrows in Figure 5 denote the resonant frequencies for an untwisted pmm beam with the same cross section, with $f = 28, 182$ and 520 Hz representing the first three natural frequencies for the direction with the lower bending rigidity and $f = 42, 275$ and 780 Hz those for the stiffer direction. Comparisons of these with the resonant peaks for the twisted beam show that twist has a larger effect at higher frequencies. The lowest resonant frequencies of both the twisted and untwisted beams were found to be essentially the same. Figure 6 illustrates the spatial variation in the amplitude ratio and phase for the resonant frequencies of 28, 192 and 560 Hz in the twisted pmm beam. The general quality of the distributions is similar to the corresponding curves for the untwisted beam however the amplitudes at the higher resonances are somewhat lower for the twisted beam.

We have also determined the variations of Young's modulus with frequency for a pmm beam and for a rectangular strip of bone machined from a dog radius. The method used is similar to that described by Bland and Lee [3]. For steady state oscillations in a linear viscoelastic material it is convenient to express the constitutive equation in terms of a complex Young's modulus which accounts for

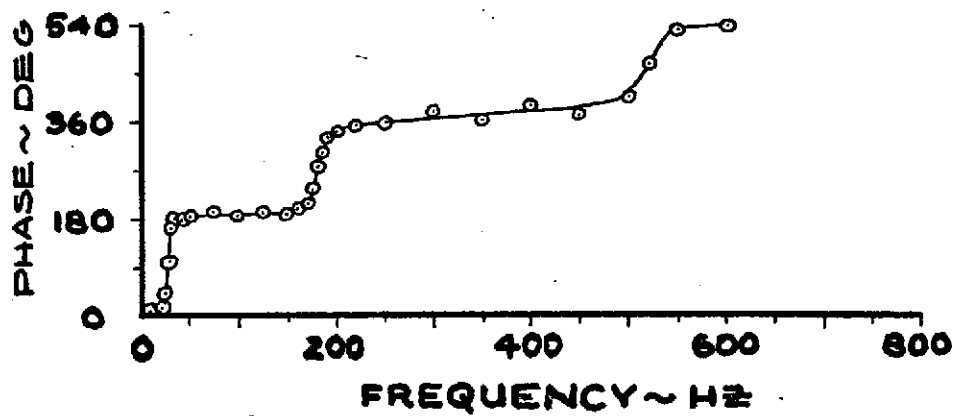
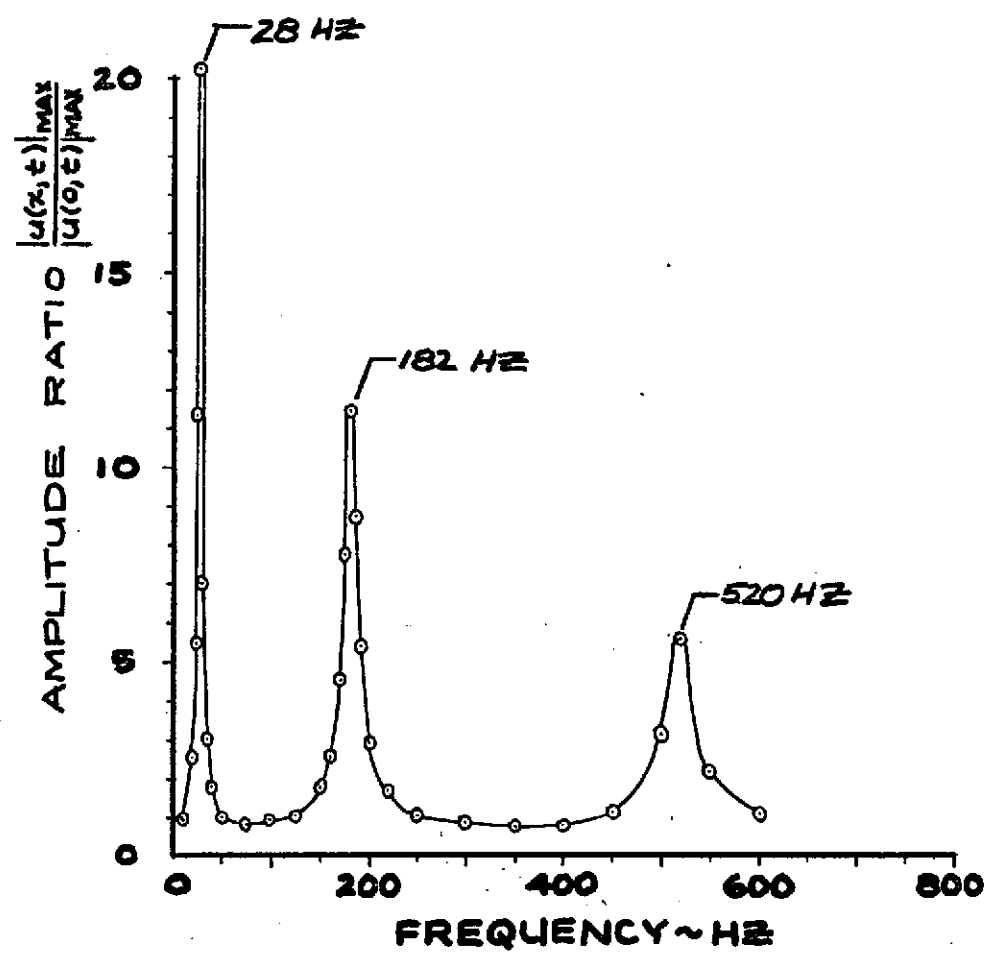


Figure 3. Amplitude ratio and phase angle for an untwisted pmm beam as a function of frequency, $x/L = 0.98$.

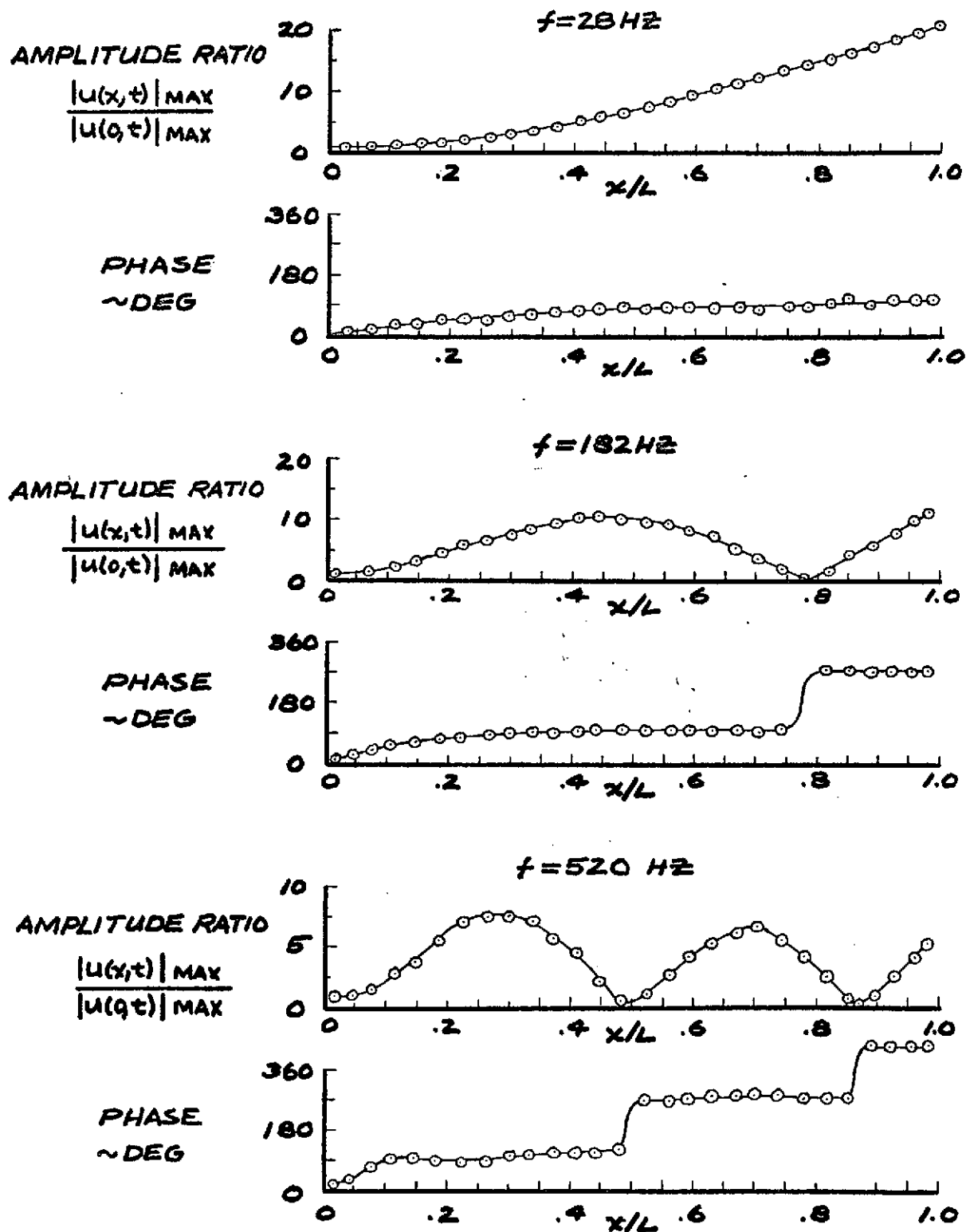


Figure 4. Spatial distributions of the amplitude ratio and phase angle for an untwisted pm beam at the first two resonant frequencies.

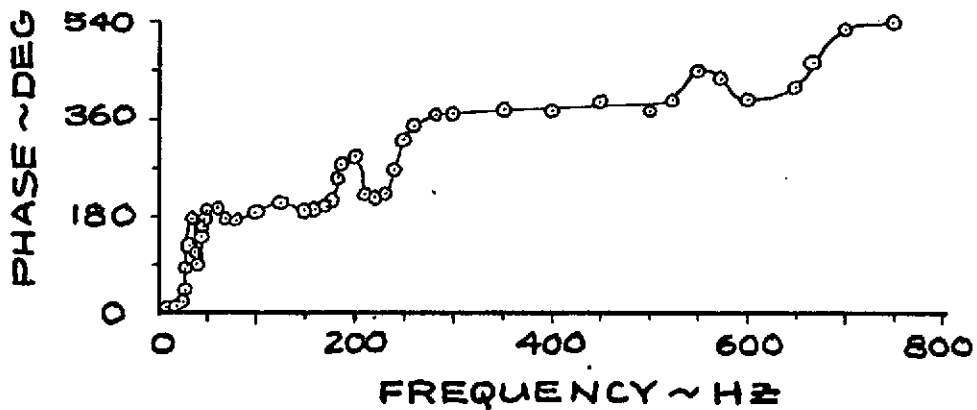
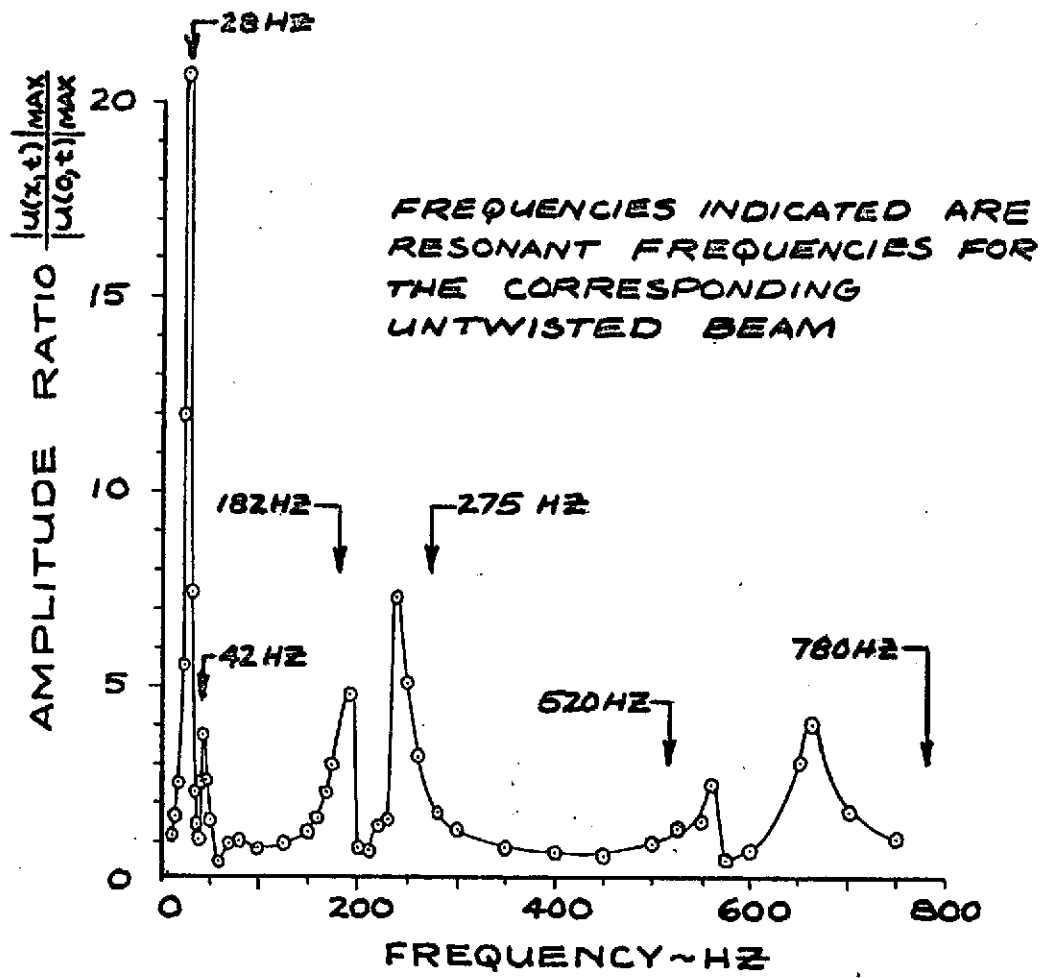


Figure 5. Amplitude ratio and phase angle for a twisted pmm beam as a function of frequency, $x/L = 0.96$.

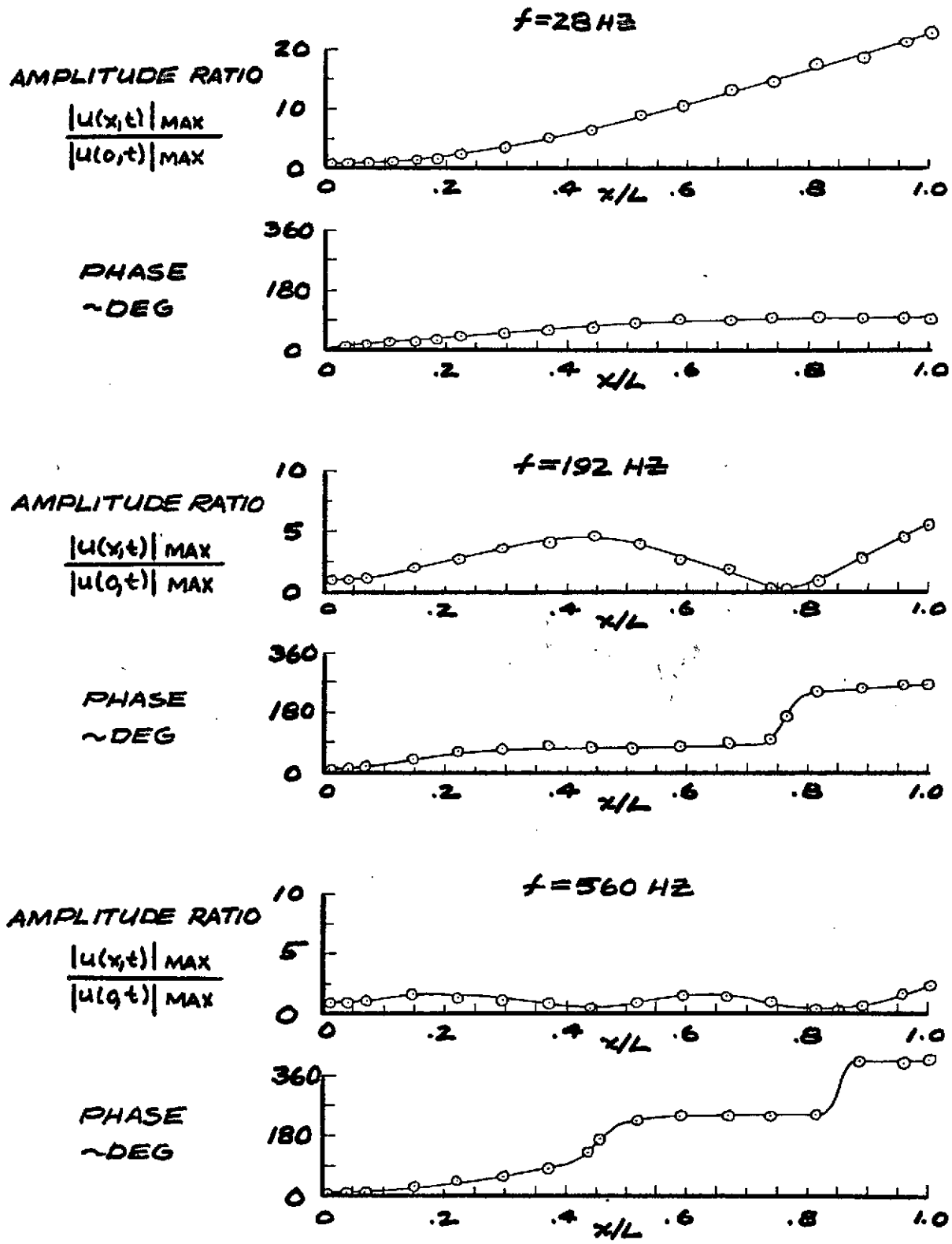


Figure 6. Spatial distributions of the amplitude ratio and phase angle for a twisted pmm beam at three resonant frequencies.

the fact that in such materials the stresses and strains are generally out of phase. Writing the complex elastic modulus as

$$E(\omega) = E_0(\omega) [1 + i\delta(\omega)]$$

we can determine $E_0(\omega)$ and $\delta(\omega)$ in a convenient manner by varying the beam length to obtain a range of resonant frequencies. According to Bland and Lee [3] we have approximately

$$E_0 = \frac{\rho A}{I} \left(\frac{L}{K_n} \right)^4 \omega^2 \left(1 - \frac{6c_n^2}{K_n^2 A_L^2} \right) \quad (2a)$$

$$\delta = \frac{4c_n}{K_n A_L} \left(1 + \frac{5c_n^2}{K_n^2 A_L^2} \right) \quad (2b)$$

A_L = amplitude ratio for the free end at the resonant peaks

ω = circular frequency

ρA = mass per unit length

I = area moment of inertia of the cross section

c_n, K_n are constants depending on the number of the mode of vibration:

vibration mode	K_n	c_n
First	1.875	0.734
Second	4.694	1.018
Third	7.854	0.999

The above equations used to calculate the complex modulus are valid for uniform linearly viscoelastic cantilever beams if $\delta \leq 1/2$ and if shear deformations and rotatory inertia effects are negligible.

Figure 7 shows the complex modulus vs. frequency as measured for pmm. The points illustrated are the results obtained from our experiments, while the dotted line depicts the modulus for pmm as measured by Koppelman [4]. Differences between our measurements and those by Koppelman may be due to actual differences in the specimens tested. The real part of the elastic modulus for pmm slowly increases with frequency while the ratio of the imaginary part to the real part decreases with frequency.

The complex elastic modulus for a dehydrated bone strip is given in Figure 8 as a function of frequency. The specimen was obtained from the central portion of a dog radius and it was machined to have a rectangular cross section with a width of 0.43 cm and a thickness of 0.21 cm. The length was varied between 3.0 and 7.5 cm by clamping the strip at different stations with the circles representing measurements obtained when the distal end (wrist end) of the strip was clamped and the triangles when the proximal end was fixed. Differences between the measurements obtained by clamping opposite ends can be attributed to inhomogeneities in the

$$E(\omega) = E_0(\omega) [1 + i \delta(\omega)]$$

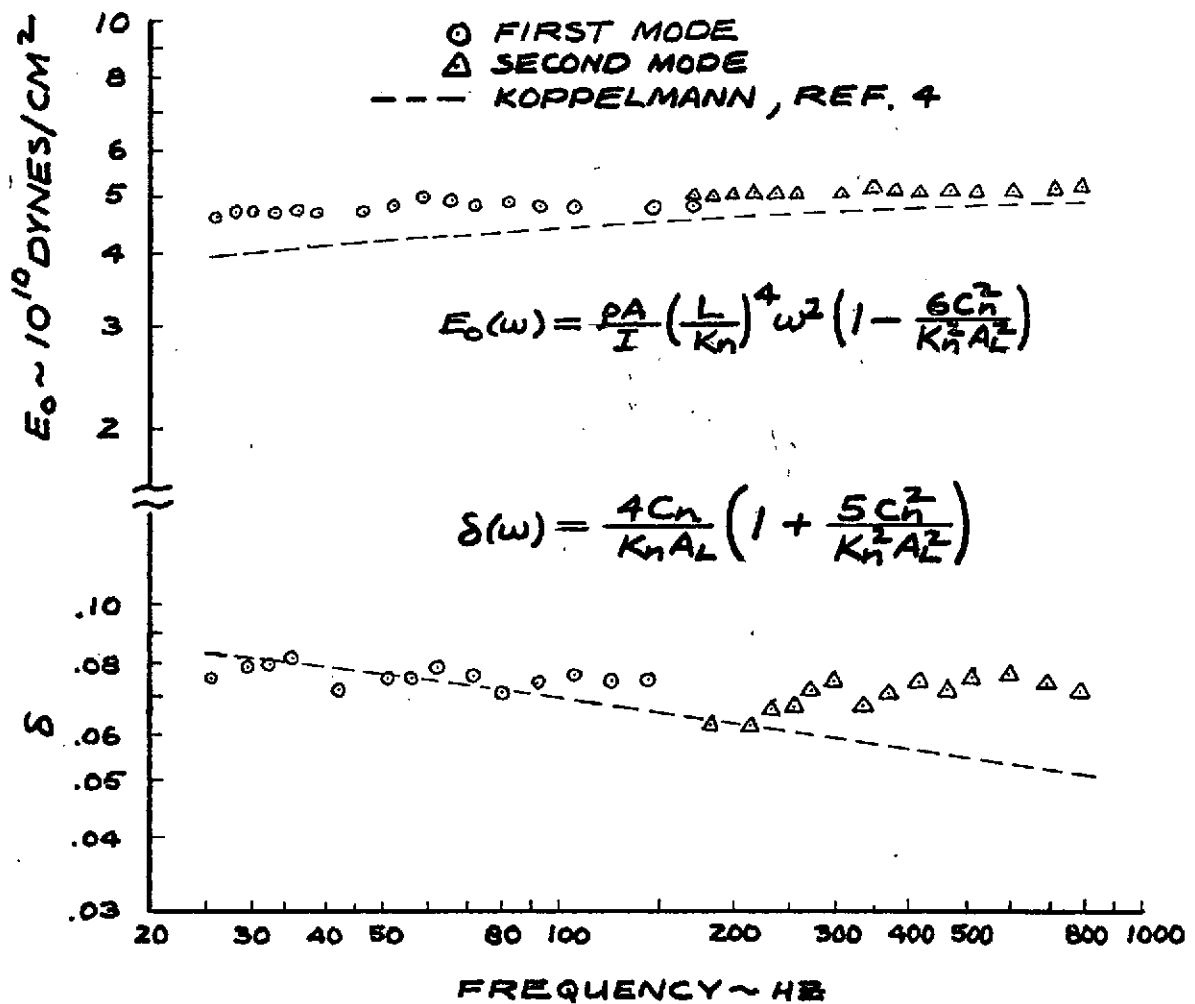


Figure 7. The complex elastic modulus $E(\omega)$ as a function of frequency for pmm.

$$E(\omega) = E_0(\omega)[1 + i\delta(\omega)]$$

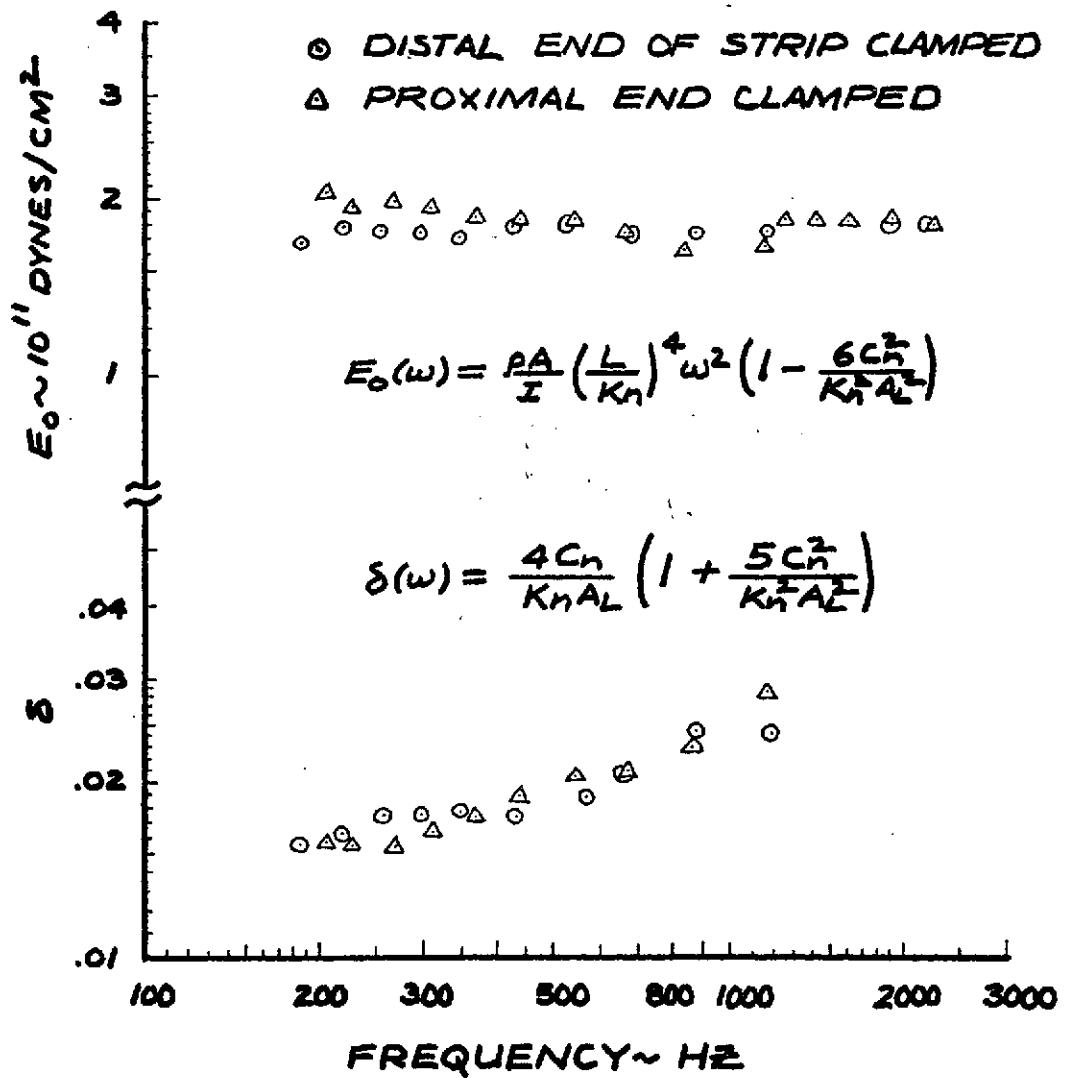


Figure 8. The complex elastic modulus $E(\omega)$ as a function of frequency for a dehydrated bone strip machined from a dog radius.

specimen. The real part of the elastic modulus for the bone strip is relatively independent of frequency while the ratio of the imaginary to the real part increases with frequency. These results for the bone strip will later be compared with measurements made on the whole bone prior to machining.

STATIC AND DYNAMIC DISPLACEMENT PATTERNS FOR EXCISED DOG RADII

Static Bending

Static deflections of excised dog radii were measured to allow for comparisons with the forced vibration response and to examine the importance of shear deformations in whole bones. In Figure 9a the lateral displacement at a number of stations is shown as a function of the lateral load. As before, the x axis is directed along the longitudinal centerline of the bone with its origin at the clamped end and L denotes the distance from the clamped support to the free end of the bone. The lateral loads inducing bending were applied near the free end at the station $x/L = 0.98$. Anatomically the applied loading simulates in part a forward extended front leg bearing weight. The data suggest that for the range of loadings considered the displacement at all stations was a linear function of the applied load. By plotting the slopes of the deflection vs. load lines as a function of x/L the deformation shape defined by the circles in Figure 9b is obtained. The curve shown in Figure 9b is the deformation shape for a uniform cantilever beam of the same length as the bone, with a bending rigidity of $EI = 8.1 \times 10^9$ dynes-cm² and an infinite shearing rigidity. Since the curve fits the data points quite well the effects of inhomogeneities and shear deformities appear to be quite small for static bending.

Free Vibration

Free vibrations of a dehydrated dog radius mounted as a cantilever are shown in Figure 10. The bone was initially loaded with a 200 gm weight in the same manner as was done for the static bending tests. The two displacement traces shown in Figure 10 are for the free end of the bones, the lower horizontal trace being the initial static deflection. The horizontal time scale is 10 msec per division and each vertical division is 0.010 cm displacement. Approximating the free vibration curve as an exponentially decaying sinusoidal oscillation, we have

$$u(L, t) = U_0 e^{i\omega t}$$

where ω is complex, i. e.

$$\omega = 2\pi f + i\gamma$$

Then

$$u(L, t) = U_0 e^{-\gamma t} e^{2\pi i f t}$$

The real part of the frequency can be obtained by measuring the average period of the oscillations. We find $f = 187$ Hz. The attenuation coefficient γ can be calculated from

$$\gamma = \frac{1}{t_m - t_n} \ln \frac{A_n}{A_m}$$

where $A_n = A_0 e^{-\gamma t_n}$ is the maximum amplitude at the time t_n and A_m that for $t = t_m$. This gives a value of $\gamma = 18$ for the free vibration. While we can

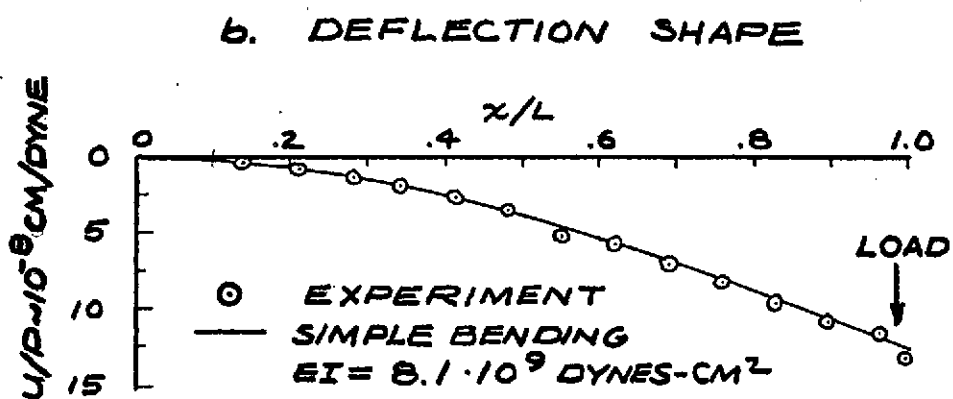
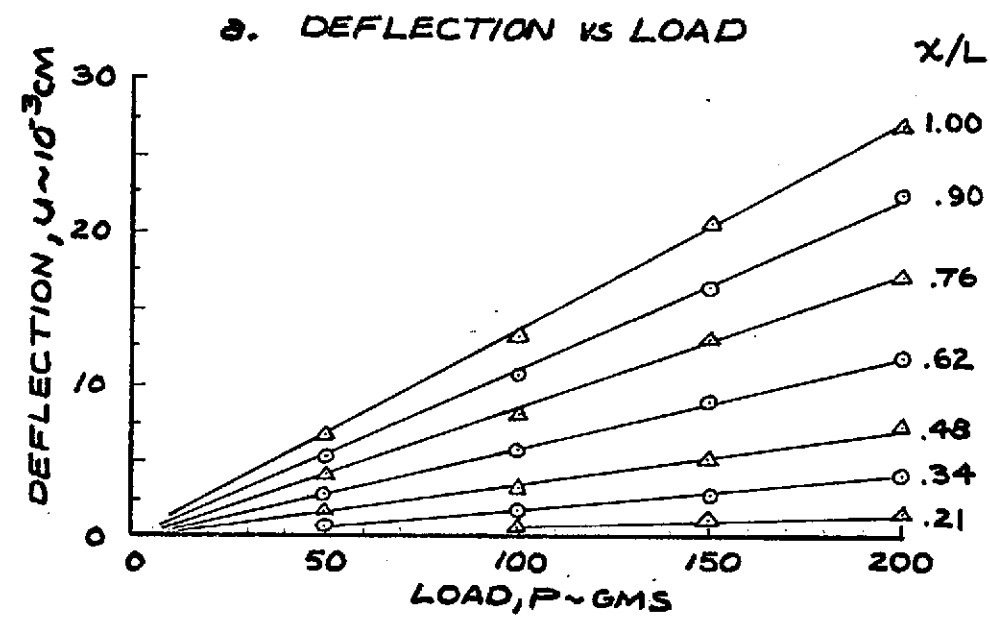
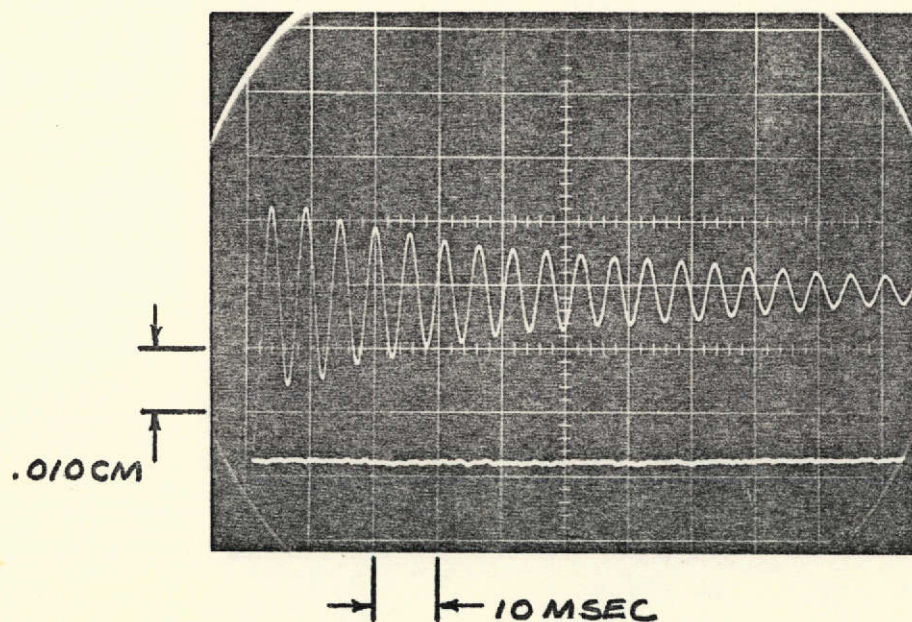


Figure 9. Static bending response of a dehydrated dog radius.



$$u(L,t) = U_0 e^{(2\pi i f - \gamma)t}$$

$$f = 187 \text{ Hz}$$

$$\gamma = 18$$

Figure 10. Free vibration response of a dehydrated dog radius, $x/L = 1.0$.

compute a complex modulus from f and γ it is expected to be somewhat different from that given by the forced vibration response since it corresponds to a complex frequency. In steady state oscillations the frequency is real.

Forced Vibrations

Forced vibrations were excited in the dog radii in the same direction as the static deflection patterns mentioned above. In these tests care was taken to keep the amplitude of the motion small enough so that the amplitude of the bone motion was a linear function of the clamped end displacement; the maximum shaker displacement used was .010 cm peak-to-peak. Nonlinear effects were most noticeable at the first resonant frequency where the amplitude of the free end displacement is very large compared to the clamped end motion. The amplitude ratio and phase angle for a dehydrated dog radius are shown as a function of frequency in Figure 11. The bone used here is the same as that for which the static bending and free vibration results were shown. We notice strong resonances at 189 Hz and 1000 Hz. The ratio of the second to first resonant frequency is 5.3, and as such deviates from the classical value of 6.27 for a uniform slender cantilever beam. The first resonant frequency of 189 Hz compares favorably with the real part of the frequency found for free vibrations. Between the two large resonance peaks there is a small intermediate peak at 275 Hz and at this frequency the phase angle curve shows a depression. This intermediate peak appears to be due to the twist in the dog radius since the response of the twisted pmm beam shown in Figure 5 exhibits similar features. If the bone is rotated 90 degrees and vibrated, a strong resonance occurs at 275 Hz. The spatial distribution of the response at the first two resonant frequencies is given in Figure 12. Again it should be noted that the amplitude ratio distribution does not represent the displacement shape at a particular time because maximum amplitudes for different stations occur at different times. From the first resonant frequency of $f = 189$ Hz and the amplitude ratio for the free end of $A_L = 85$ we can estimate an effective Young's modulus for the whole bone using equations (2). At this point it is important to stress that the effective modulus obtained in this manner is an average property for the whole bone since it is based on uniform beam theory. The inhomogeneities in the bone render the analysis not strictly correct. For the dog radius tested we found approximately

$$\rho A = 1.59 \text{ gm/cm}$$

$$I = 0.021 \text{ cm}^4$$

$$L = 14.5 \text{ cm}$$

and

$$E_{\text{eff}} = 3.8(1+0.02i) \times 10^{11} \text{ dynes/cm}^2$$

In the static bending test we obtained an effective bending rigidity of $(EI)_{\text{eff}} = 8.1 \times 10^9 \text{ dynes/cm}^2$. Using the above value of I , the static bending test gives a value of $E_{\text{eff}} = 3.86 \times 10^{11} \text{ dynes/cm}^2$ for the effective Young's modulus. The mass per unit length used in the above calculations was obtained by weighing the whole bone and dividing by the length and hence represents an average for the whole bone.

We previously showed the results obtained for the complex modulus as a function of frequency for a strip of bone machined from the central portion of a dog radius. Prior to the machining operation two sets of resonant frequency measurements were done on the specimen. First, the whole bone was tested and then a shortened version of the same bone with a portion of the free end cut off. The results are summarized in the following table.

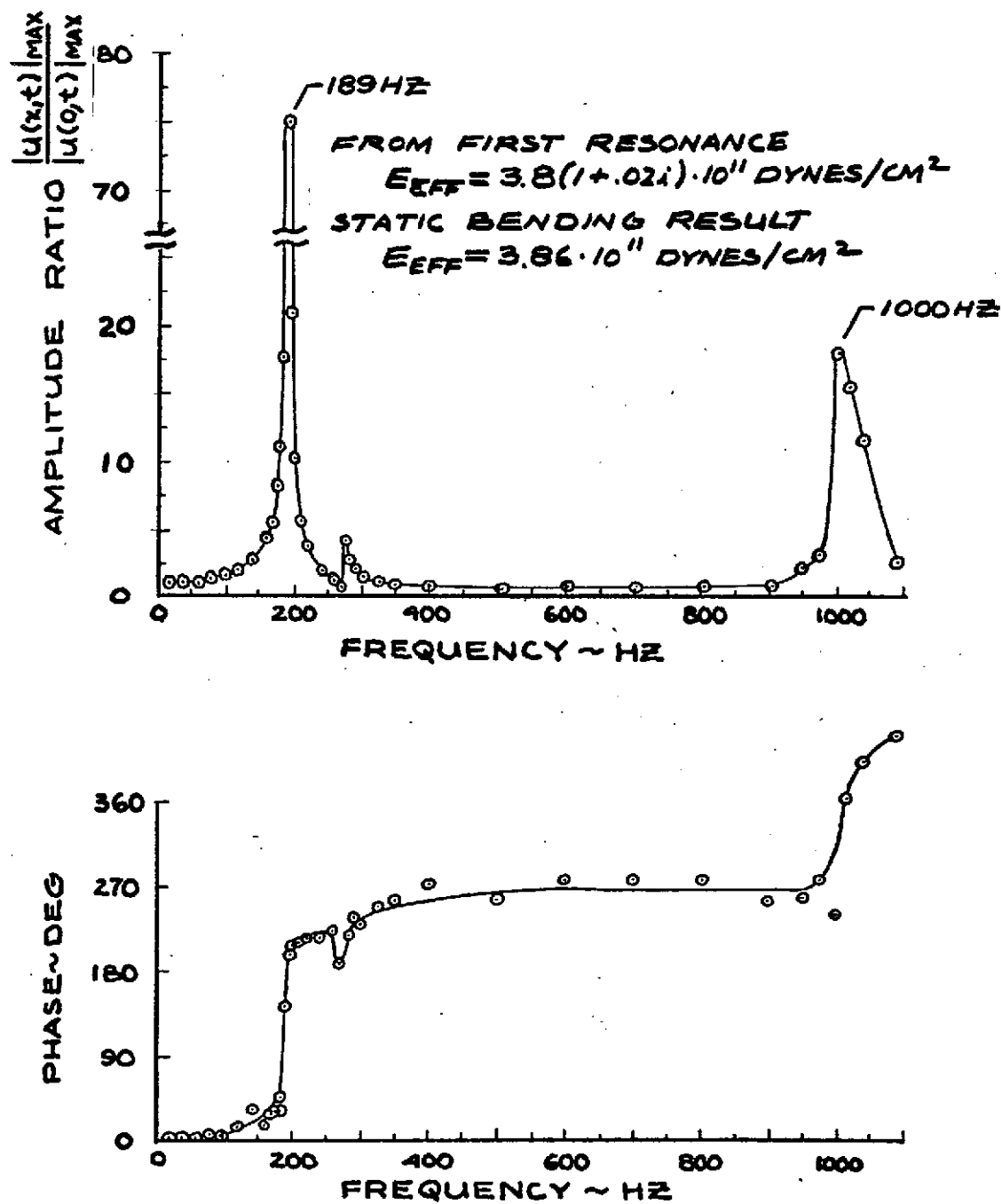


Figure 11. Amplitude ratio and phase angle for a dehydrated dog radius as a function of frequency, $x/L = 0.94$.

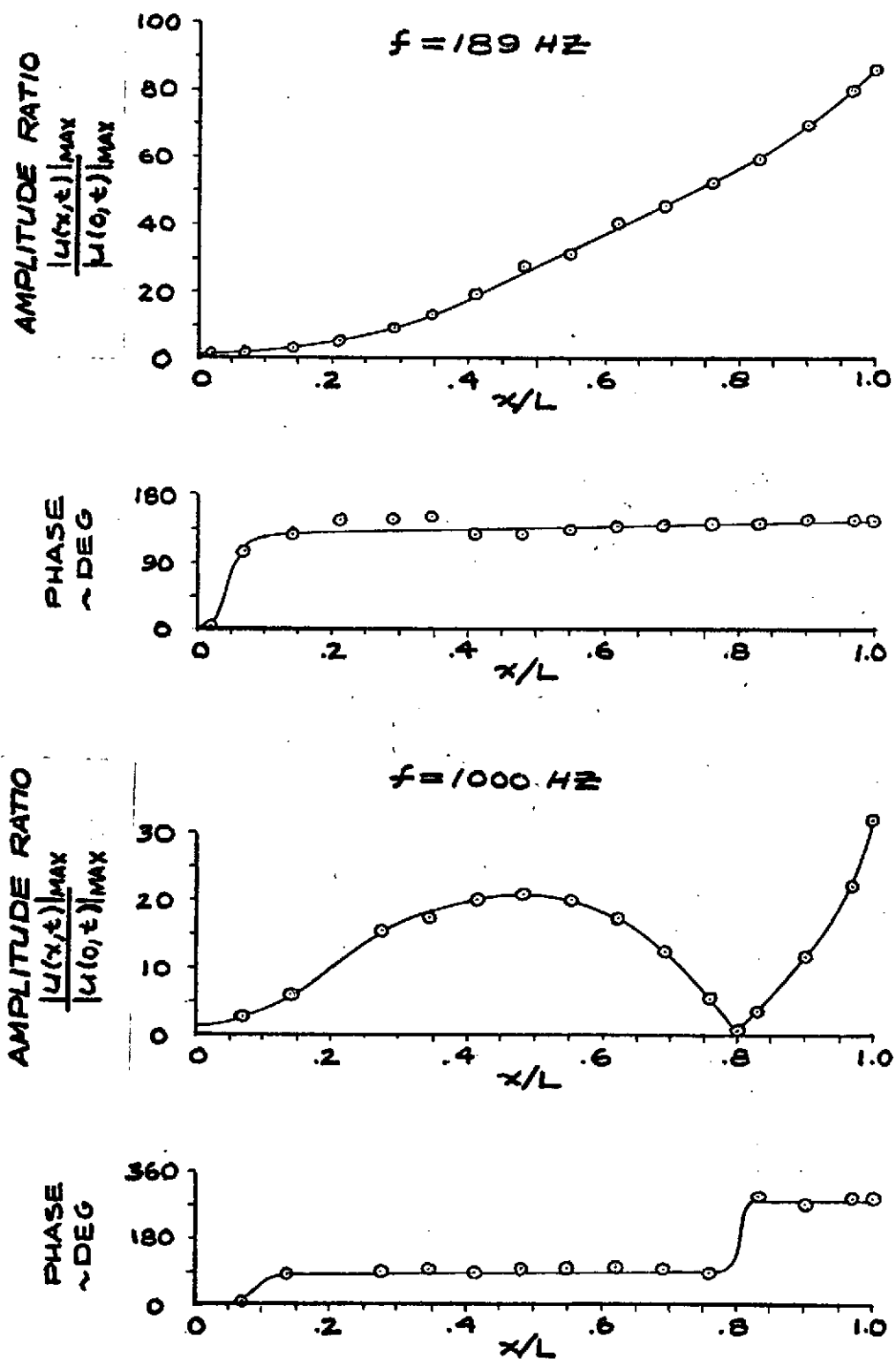


Figure 12. Spatial distributions of the amplitude ratio and phase angle for a dehydrated dog radius at the first two resonant frequencies.

Length L ~ cm	First Resonance f ₁ ~ Hz	Amplitude Ratio A _L	Mass/Length ρA ~ gm/cm	E _o x 10 ⁻¹¹ dynes cm ²	δ
16.4	158	60	1.92	2.21	.026
13.5	240	54	1.91	2.25	.029

The above values for the elastic modulus data are slightly higher than those obtained for the machined dehydrated strip.

Forced vibration tests were also done on dog radii preserved in Ringer's solution. A typical amplitude ratio of such a wet bone is shown in Figure 13. The corresponding resonant frequencies were found to be 128 Hz and 765 Hz. After dehydration these frequencies increased to 158 and 996 Hz respectively. This increase is mainly due to a reduction in the mass per unit length caused by dehydration. The effective Young's modulus, calculated from the resonant frequency and amplitude ratio data for the wet sample, is $E_{\text{eff}} = 2.1(1 + 0.07i) \times 10^{11}$ dynes/cm² at 128 Hz. For this specimen, when dehydrated, we found an effective modulus of $E_{\text{eff}} = 2.2(1 + 0.03i) \times 10^{11}$ dynes/cm². Dehydration reduces the imaginary part of the effective Young's modulus and thus the viscoelastic damping.

DISCUSSION AND CONCLUSIONS

Our experimental data indicate that the effects of viscoelastic damping and natural twist of the principal axes of inertia on the resonant frequencies are small; the amplitude ratio and phase distributions, however, are noticeably affected. While the influence of shear on the lowest natural frequency also appears to be small it seems to produce, in some cases, a second eigenfrequency which is as much as 20% below the values anticipated on the basis of classical theory. If this discrepancy is exclusively due to shear, the bone material in such cases is highly anisotropic and has a shear modulus which is of the order $E/30$. An elastic modulus calculated from the first resonance data for forced vibration, using uniform beam theory, agrees well with the static bending results. Since the experimental data shows evidence of both physical and geometric nonuniformities, the calculated elastic moduli are to be interpreted as effective moduli which represent weighted averages for the whole bone.

AMPLITUDE RATIO RESPONSE WET DOG RADIUS

$$x/L = 0.99$$

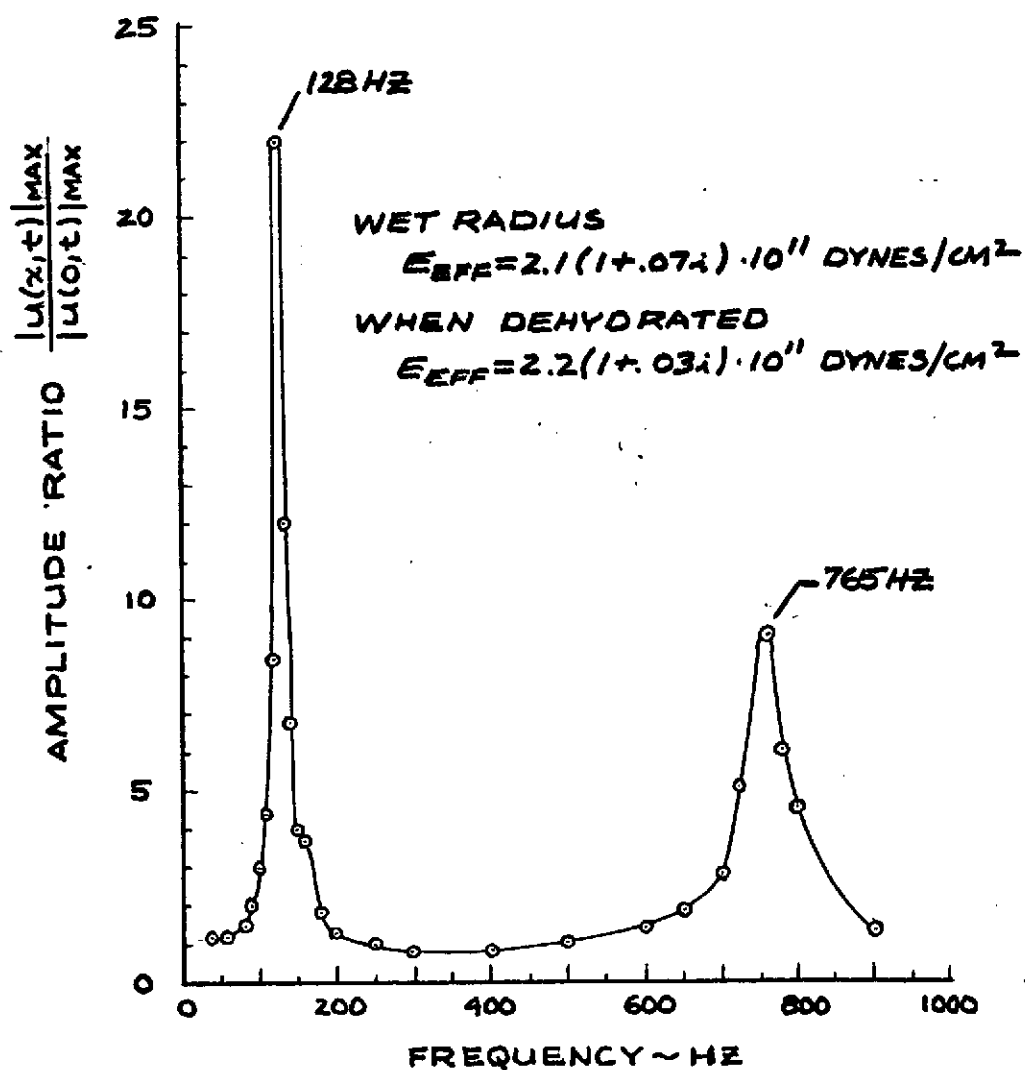


Figure 13. Amplitude ratio for a wet dog radius (preserved in Ringer's solution) as a function of frequency, $x/L = 0.99$.

REFERENCES

1. Cameron, J.R., Jurist, J.M., Sorenson, J.A. and Mazess, R.B.: New methods of skeletal status evaluation in space flight. *Aerospace Med.* 40(10):1119-1122, 1969.
2. Timoshenko, S. and Young, D.H.: *Vibration Problems in Engineering*. D. Van Nostrand Co., Princeton, N.J., ed. 3, 1955.
3. Bland, D.R. and Lee, E.H.: Calculation of the complex modulus of linear viscoelastic materials from vibrating reed measurements. *J. App. Phy.* 26(12):1497-1503, 1955.
4. Koppelman, Von Jan: Über das dynamisch-elastische Verhalten hochpolymerer Stoffe. *Kolloid Zeitschrift* 144:12-41, 1955.

ACKNOWLEDGEMENTS

The work described has been supported by NASA Grant NGL 05-020-223 and by NIH Predoctoral Fellowship 5 F01 GM 43015.